Geophys. J. Int. (2009) doi: 10.1111/j.1365-246X.2009.04163.x

Geodetic observations of the ongoing Dabbahu rifting episode: new dyke intrusions in 2006 and 2007

Ian J. Hamling,[1] Atalay Ayele,[2] Laura Bennati,[3] Eric Calais,[3] Cynthia J. Ebinger,[4] Derek Keir,[1] Elias Lewi,[2] Tim J. Wright[1] and Gezahegn Yirgu[5]

[1] *School of Earth and Environment, University of Leeds, Leeds,* LS2 9JT, *UK. E-mail: i.hamling@see.leeds.ac.uk*
[2] *The Geophysical Observatory, Addis Ababa University, Addis Ababa, Ethiopia*
[3] *Department of Earth and Atmospheric Sciences, Purdue University, IN, USA*
[4] *Department of Earth and Environmental Sciences, University of Rochester, New York, NY, USA*
[5] *Department of Earth Sciences, Addis Ababa University, Addis Ababa, Ethiopia*

Accepted 2009 February 16. Received 2009 January 14; in original form 2008 July 10

SUMMARY

A 60-km-long dyke intruded the Dabbahu segment of the Nubia–Arabia Plate boundary (Afar, Ethiopia) in 2005 September, marking the beginning of an ongoing rifting episode. We have monitored the continuing activity using Satellite Radar Interferometry (InSAR) and with data from Global Positioning System (GPS) instruments and seismometers deployed around the rift in response to the initial intrusion. These data show that a sequence of new dyke intrusions has reintruded the central and southern section of the Dabbahu segment. The first was in 2006 June and seven new dykes were emplaced by the end of 2007. Modelling of InSAR data indicates that the dykes were between 0.5 and 2 m wide, up to ∼10 km long and confined to the upper 10 km of crust. An intrusion in 2007 August was associated with a 5-km-long basaltic fissural eruption. During the new dyke injections, InSAR and GPS data show no subsidence at either of the volcanoes at the northern end of the segment, which partly fed the 2005 September dyke. Seismicity data imply that the dykes were probably fed from a source near the Ado'Ale Silicic Complex at the centre of the segment, but the lack of significant subsidence there implies that the source is very deep, or that there was minimal deflation at shallow magma sources. The new dykes are concentrated in an area where the 2005 dyke did not produce significant opening, implying that residual tensile tectonic stresses are higher in this location and are focusing the later intrusions. The sequence of dyke intrusions observed so far is similar to those seen in Iceland during the Krafla rifting episode, which lasted 9 yr from 1975 to 1984. It is likely that, with a continued magma supply, dykes will continue to be intruded until the tectonic stress is fully relieved. As observed at Krafla, eruptions are likely to become more common before the rifting episode is concluded.

Key words: Radar interferometry; Satellite geodesy; Mid-ocean ridge processes; Continental margins: divergent; Remote sensing of volcanoes; Africa.

1 INTRODUCTION

Rifting episodes, where new crust is added through the intrusion of multiple dykes in a short period of time, are known to play a key role in seafloor spreading but are seldom observed above sea level (e.g. Delaney *et al.* 1998). The most recent known examples occurred at Krafla, Northern Iceland, where a series of 20 dykes were intruded over a 9 yr period from 1975, (Einarsson & Brandsdóttir 1980; Tryggvason 1984; Buck *et al.* 2006) and in the Asal rift in 1978, where 2 m of extension was achieved following the intrusion of a dyke at a new eruptive centre (Abdallah *et al.* 1979; Cattin *et al.* 2005; Vigny *et al.* 2007). In 2005 September a 60-km-long rift segment ruptured in Northern Afar, Ethiopia, marking the beginning of an ongoing rifting episode (Wright *et al.* 2006; Yirgu *et al.* 2006; Ayele *et al.* 2007; Rowland *et al.* 2007; Ebinger *et al.* 2008).

The Afar depression, comprising the Afar triple junction, formed as a result of rifting between Africa and Arabia over the past ∼30 Myr. The three arms of the triple junction, the Red Sea, Gulf of Aden and East African rifts (Fig. 1), formed within a Palaeogene flood basalt province associated with the Afar mantle plume (Schilling *et al.* 1992; Hofmann *et al.* 1997; Ebinger & Sleep 1998), roughly coincident with the onset of rifting in the Red Sea and Gulf of Aden (Wolfenden *et al.* 2004). Low *P*- and *S*-wave velocities in the upper mantle beneath the uplifted plateaus of Arabia and NE Africa indicate that the thermal anomaly associated with the plume exists till today (Benoit *et al.* 2003, 2006; Bastow *et al.* 2008).

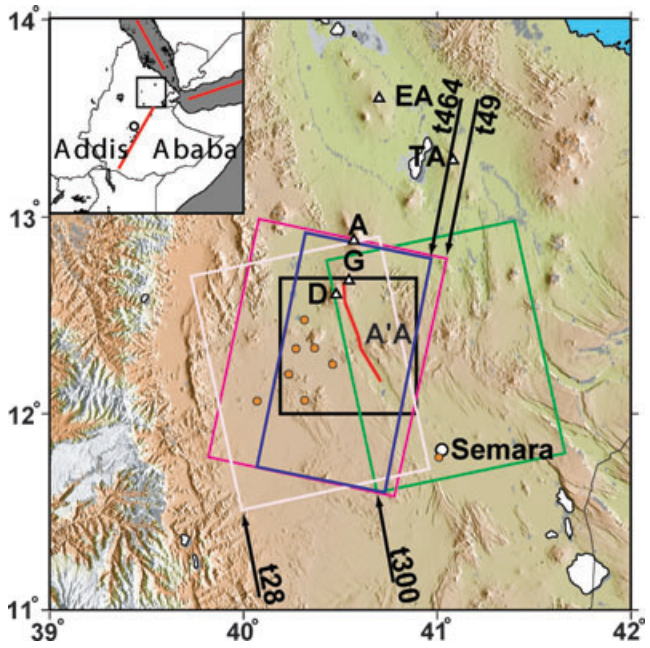

Figure 1. Colour shaded relief map of northern Afar. Main figure shows the location of the dyke (red line) intruded in 2005, Gabho (G), Dabbahu (D), Alayta (A), Ado'Ale (A'A), Tat'Ale (TA) and Erta'Ale (EA) volcanoes (white triangles) and Semara, the regional capital (white circle). The coloured boxes indicate the available InSAR coverage—tracks 28 (green box), 49 (pink box), 300 (white box) and 464 (blue box). Orange circles indicate the continuous GPS stations used in the joint inversion of InSAR and GPS data. The black box indicates the region covered by the interferograms in Figs 6–12. The Manda–Hararo segment runs from Dabbahu to Semara.

The currently-active Dabbahu segment lies within the Red Sea arm of the triple junction. Rifting in the Red Sea has progressed to seafloor spreading between ∼21°N and ∼15°N, south of which spreading is offset to the west into northern Afar. Seismic refraction and reflection studies indicate that the highly intruded and extended Afar crust varies from 18 km thick in the north to 26 km thick in the south (Berckhemer *et al.* 1975; Makris & Ginzburg 1987; Tiberi *et al.* 2005; Stuart *et al.* 2006). Geodetic and geological data suggest an average spreading rate of <20 mm yr^{-1} (Chu & Gordon 1998; Kreemer *et al.* 2005; Vigny *et al.* 2006).

Since ∼3 Ma, faulting and volcanism in Afar, have localized to ∼60-km-long, 20-km-wide axial volcanic ranges of aligned magmatic centres, similar in size, morphology and spacing to the second-order, non-transform offset segmentation of slow-spreading mid-oceanic ridges (Hayward & Ebinger 1996; Manighetti *et al.* 1998). The subaerial section of the Red Sea rift is comprized of numerous, previously mapped, magmatic segments (Hayward & Ebinger 1996). The northernmost segments of Erta'Ale and Tat'Ale are characterized by axial volcanic ranges (Barberi *et al.* 1972) (Fig. 1). To the south, the rift jumps to the west to the Alayta and Manda-Hararo segments (Fig. 1). The Dabbahu segment forms part of the larger Manda-Hararo rift segment, which, unlike the more northern magmatic segments, is characterized by a 35-km-wide depression (Rowland *et al.* 2007). Barberi & Varet (1975) state that the segment is the only place in Afar where typical mid-oceanic basalts occur. More recent geochemical analysis of Manda-Hararo basalts show both enriched and depleted light rare earth element (LREE) suggesting the involvement of two different mantle components (Barrat *et al.* 2003).

The Dabbahu rifting episode was first detected on 2005 September 14 when an earthquake of magnitude (M_b) ∼ 4.7 was recorded. In total, a swarm of 162 earthquakes (magnitude 4.1–5.2) were recorded by NEIC between September 20 and October 4, coinciding with the opening of a new 400-m-long, 80-m-wide volcanic vent on the eastern flank of Dabbahu volcano (Wright *et al.* 2006; Yirgu *et al.* 2006; Ayele *et al.* 2007; Rowland *et al.* 2007). The Geophysical Observatory at Addis Ababa University recorded nearly continuous activity between September 24 and 26 with the number of earthquakes declining on September 27 (Yirgu *et al.* 2006). An earthquake of magnitude 5.2 on September 26 occurred approximately half an hour before the onset of the volcanic eruption, according to local pastoralists. The eruption was composed of pumice, fine ash and silicic lava. Initial analysis of the erupted rhyolitic pumice indicated a felsic source at a depth of <6 km (Wright *et al.* 2006). Surface deformation estimated from radar interferometry indicated a maximum horizontal opening of 8 m perpendicular to the rift (Wright *et al.* 2006; Ayele *et al.* 2007). A maximum uplift of ∼1.5 m occurred on both rift flanks with respect to the far field and extended along most of the segment. A 2–3-km-wide central zone subsided by up to 2 m, with a further 2–3 m of subsidence occurring around Dabbahu and Gabho volcanoes at the northern end of the segment. The observed surface deformation and seismicity were in accordance with the injection of a 60-km-long dyke, between 2 and 9 km depth along the length of the segment (Wright *et al.* 2006; Yirgu *et al.* 2006; Ayele *et al.* 2007; Rowland *et al.* 2007).

Deformation, at rates of a few cm per month, was observed around the rift segment in the months following the initial intrusion (Ebinger *et al.* 2008; Section 2.2). Seismicity suggests that this may result from continued magma injection. The deformation style changed dramatically on 2006 June 17 when a new dyke was intruded in the vicinity and to the south of the Ado'Ale volcanic complex—a dissected, central silicic centre 30 km south of Dabbahu volcano (Keir *et al.* 2008). By the end of 2007, a total of seven new dykes had been intruded into the Dabbahu segment. Here we present a number of ascending and descending interferograms from 2006 June to 2007 November covering each of the new dykes. We use elastic modelling of InSAR and GPS data to determine the geometry and amount of opening for each event, compare the results with the 1975–1984 Krafla rifting episode and provide further evidence for the presence of a deep magma source below the centre of the Dabbahu rift segment.

2 METHODS

2.1 InSAR data

Satellite Radar Interferometry (InSAR) is a widely used technique for monitoring deformation of the Earth's surface. By differencing the phase from two radar images acquired at different times, maps of range change between the radar and ground can be obtained with centimetre precision (Massonnet & Feigl 1998). Following the 2005 September rifting episode regular Advanced Synthetic Aperture Radar (ASAR) acquisitions have been acquired over the Dabbahu magmatic segment using ESA's Envisat satellite (Fig. 2). All of the interferograms have been processed using the JPL/Caltech ROI_PAC software (Rosen *et al.* 2004). Topographic corrections were made using a 3″ (90 m) digital elevation model (DEM) generated by the NASA Shuttle Radar Topography Mission (Farr & Kobrick 2000). Interferograms are filtered using a power spectrum filter (Goldstein & Werner 1998) and unwrapped using the branch

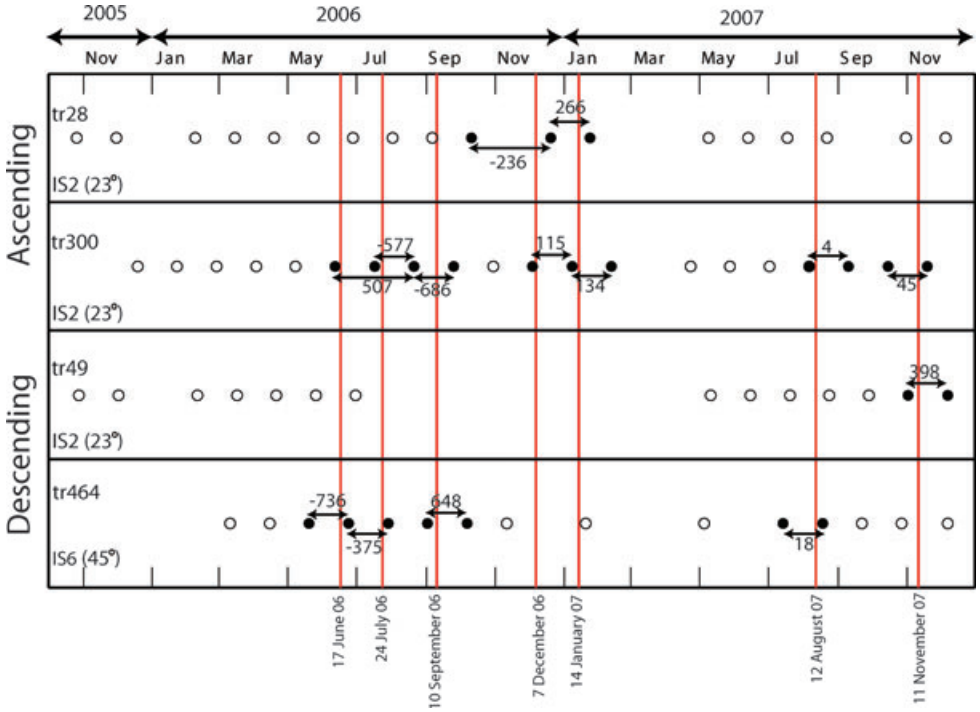

Figure 2. Time line from 2005 October 1 to 2007 December 31, showing available ASAR acquisitions. Red lines indicate the intrusion of a dyke into the segment. Circles indicate the available ASAR images for each of the four tracks, the filled circles are the images used for this study. The black arrows indicate the ASAR pairs used to construct each interferogram with the perpendicular baseline (m) labelled.

cut algorithm (Goldstein *et al.* 1988). The unwrapped interferograms are checked for any unwrapping errors and corrected for, where necessary. In cases where ambiguities could not be reliably determined, we removed the ambiguous phase from the unwrapped interferograms. Where data exist, and perpendicular baselines allow, interferograms are formed with the shortest possible time span, which for Envisat is 35 d (Fig. 2). Fortunately, coherence in the Afar region is generally high due to the arid environment, and interferograms with perpendicular baselines as large as 600 m remain coherent. Although conditions are arid, water vapour from the Red Sea and Gulf of Aden cause an average far field noise of 20 mm.

2.2 GPS data

In addition to the InSAR data, continuously recording GPS data from up to 11 sites, installed in and around the rift segment in response to the 2005 dyke injection, were available covering the 2006–2007 dyke sequence (Figs 1 and 5h).

In a first step, we processed phase and pseudo-range GPS data in single-day solutions using the GAMIT software (King & Bock 2005). We solved for station coordinates and phase ambiguities using doubly differenced GPS phase measurements. We applied azimuth and elevation dependent absolute antenna phase centre models, following the table recommended by the IGS. We implemented the reference frame by tightly constraining the GPS orbits and IERS earth orientation parameters to the final IGS values and map site positions with respect to site DA60 (Fig. 3).

With the exception of the sites located at the volcanoes—DABB and GABH—most of the sites show steady long-term westward velocities, likely to be the result of long term relaxation following the 2005 September intrusion (Fig. 3). Sites nearest the rift also show sudden displacements on the dates of dyke injections. To calculate the size of these jumps, we modelled site positions as the sum of (1) a linear term representing a long-term (constant) velocity, (2) additive shifts at the time of dyke intrusions and (3) an annual and semi-annual periodic term representing seasonal effects not modelled in the GPS data analysis. The model equation is

$$y = at + b + \sum_{i=1}^{n} c_i H(t_i) + d\sin(2\pi t) + e\cos(2\pi t) + f\sin(4\pi t) + g\cos(4\pi t) \quad (1)$$

where a, b, c_i, d, e, f and g are estimated by inverting the site position data y using a singular value decomposition scheme. $H(t_i)$ is the Heaviside step function that shifts from null to unity at the time t_i of the ith dyke intrusion, where t measures time, in years, from the beginning of GPS observations in 2006 (Press *et al.* 1986). We then use the modelled site positions corrected for the annual and semi-annual terms to compute site displacement between the time of the two SAR scenes that compose each interferogram.

2.3 Elastic dislocation modelling

2.3.1 Uniform opening model

Initially, each dyke was modelled as a rectangular dislocation in an elastic half-space, after the formulations of Okada (1985). The 3-D displacements calculated by the model are projected into the satellite line of sight (LOS) and solutions are found that minimize the square misfit between the observed and calculated LOS displacements (Wright *et al.* 1999). To make the inversion possible, the InSAR data are first subsampled using a Quadtree algorithm (e.g. Jónsson *et al.* 2002), which reduces the number of data points from $\sim 10^7$ to $\sim 10^3$. A hybrid Monte Carlo, downhill simplex inversion is used to determine a set of parameters with minimum square

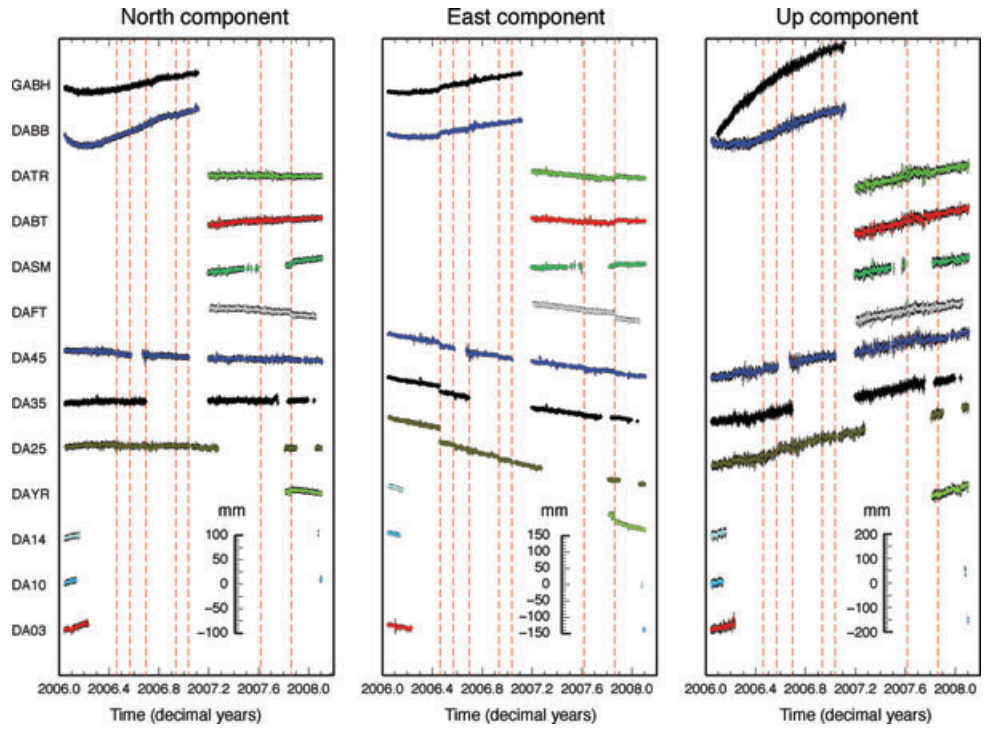

Figure 3. Position time-series at continuous GPS sites. Site names are listed each panel and is different for each of the north, east and up components. Red dashed line indicate the time of dyking events. Location of each of the GPS stations is shown in Fig. 5(h).

Table 1. Uniform opening model outputs for each of the new dykes (see Section 2.3.1 for details).

Date	Length (km)	Strike (°)	Max Opening (m)	Dip (°)	rms (mm)
June 2006	8.2 ± 0.4	335.4 ± 2.5	1.9 ± 0.1	89.9 ± 0.1	27
July 2006	9.9 ± 0.3	332.5 ± 0.6	4.0 ± 0.7	87.7 ± 1.1	38
September 2006	8.3 ± 1.6	330 ± 2	1.5 ± 0.4	89 ± 1.6	36
December 2006	8.2 ± 0.4	335.3 ± 2.5	1.9 ± 0.1	89.9 ± 0.1	50
January 2007	8.2 ± 0.4	331.8 ± 0.6	1.6 ± 0.1	89.9 ± 0.1	20
August 2007	9.1 ± 0.1	334.9 ± 1.3	1.6 ± 0.1	89.9 ± 1.2	45
November 2007	11.6 ± 0.3	331.2 ± 1.5	1.6 ± 0.1	87.9 ± 0.9	30

misfit (Wright *et al.* 1999). Using the InSAR data we solve for the position, dip and strike of the rectangular dislocation, its length and depth extent and the opening displacement, which is constant and normal to the dyke. Parameter uncertainties are calculated using a Monte-Carlo simulation in which correlated noise is added to the data (Wright *et al.* 2003; Parsons *et al.* 2006). For each interferogram, the noise is estimated by fitting covariance functions to phase data away from the dyke. Assuming this is representative of the atmospheric noise in the deforming area, the distribution of model parameters provides an estimate of their uncertainty.

The models provide useful constraints on the geometry of each of the dykes (Table 1). Despite the relatively poor misfit between predicted and observed displacements (20 mm < rms < 50 mm), we were able to use the data to determine the location of the surface trace for each of the dykes. Fig. 4 shows a density plot showing the location of the 100 best fitting dyke models for all seven of the post 2005 September dyke intrusions. The grid is divided into 1 × 1 km squares; each time a dyke passes through a patch, a counter is incremented by 1. The patches with the highest density of intersections are plotted with darker colours. The preferred locations for the dykes form a narrow NW–SE, ∼25-km-long cluster, offset by ∼2 km toward the north, and all lie within the subsiding zone associated with the 2005 September intrusion. The inverted dyke locations are consistent with the reintrusion of the September 2005 dyke plane, within uncertainties.

2.3.2 Distributed opening model

To improve the fit to the data and make the model more realistic, we next solved for a distributed opening model. The extent and shape of the dyke is determined from the uniform opening models described in Section 2.3.1, and the location of the dyke is shown by the red dashed line in Fig. 4. Field observations indicate that existing faults are reactivated after new dyke intrusions (Rowland *et al.* 2007). In the model, a generalized fault geometry has been traced from a DEM. Faults extend to a depth of 2 km dipping at 65 ° (black lines in Fig. 4) and were discretized into 1 km × 2 km patches along strike and downdip, respectively. The dyke is assumed to be vertical as uniform opening models indicate that the dykes all dip within 3° of the vertical. It is ∼75 km long and is fixed to a depth range of 0–10 km and has been divided into 750, 1 × 1 km patches. The northern 25 km of the model uses the fault and dyke geometry of Wright *et al.* (2006). Displacement along the dyke is normal to the dislocation plane and fault slip is pure normal dip-slip. The

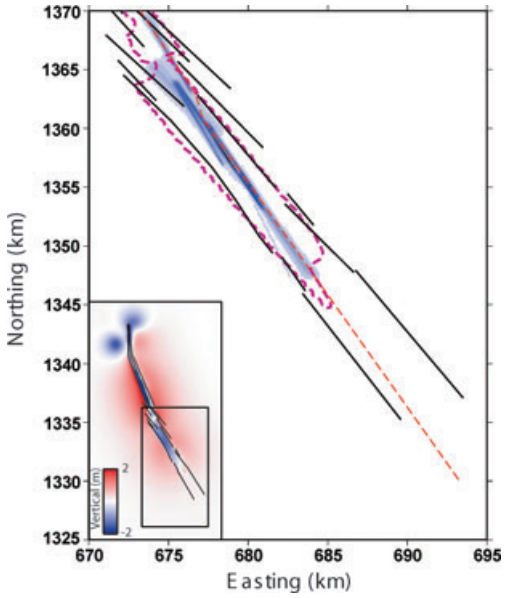

Figure 4. Density plot of the set of best fitting dykes for the seven post 2005 intrusions, black lines show the location of normal faults traced from DEM. Dashed purple line is the outline of the area of subsidence associated with the 2005 September intrusion (Wright *et al.* 2006; Rowland *et al.* 2007). The dashed red line is the chosen simplified geometry for the distributed opening model described in Section 2.3.2 The subplot shows the modelled vertical displacements from the 2005 September intrusion. Coordinates are in UTM Zone 37.

dyke opening model, **m**, for the specified geometry is determined by solving the following equation:

$$\begin{pmatrix} \mathbf{A_{asc}} & \mathbf{x} & \mathbf{y} & 1 & 0 & 0 & 0 & 0 & 0 & 0 \\ \mathbf{A_{dsc}} & 0 & 0 & 0 & \mathbf{x} & \mathbf{y} & 1 & 0 & 0 & 0 \\ \mathbf{A_{gpsx}} & 0 & 0 & 0 & 0 & 0 & 0 & 1 & 0 & 0 \\ \mathbf{A_{gpsy}} & 0 & 0 & 0 & 0 & 0 & 0 & 0 & 1 & 0 \\ \mathbf{A_{gpsz}} & 0 & 0 & 0 & 0 & 0 & 0 & 0 & 0 & 1 \\ \kappa\nabla^2 & 0 & 0 & 0 & 0 & 0 & 0 & 0 & 0 & 0 \end{pmatrix} \begin{pmatrix} \mathbf{m} \\ a_{asc} \\ b_{asc} \\ c_{asc} \\ a_{dsc} \\ b_{dsc} \\ c_{dsc} \\ c_{gpsx} \\ c_{gpsy} \\ c_{gpsz} \end{pmatrix} = \begin{pmatrix} \mathbf{d_{asc}} \\ \mathbf{d_{dsc}} \\ \mathbf{d_{gpsx}} \\ \mathbf{d_{gpsy}} \\ \mathbf{d_{gpsz}} \\ 0 \end{pmatrix}, \quad (2)$$

where $\mathbf{A_{asc}}$, $\mathbf{A_{dsc}}$, $\mathbf{A_{gpsx}}$, $\mathbf{A_{gpsy}}$ and $\mathbf{A_{gpsz}}$ are a set of matrices representing Green's functions for the ascending and descending interferograms, GPS displacements in the x, y and z directions, which, multiplied by **m**, produce the model displacements at the observation points, **x** and **y**, using the elastic dislocation formulation of Okada (1985); ∇^2 is the finite difference approximation of the Laplacian operator, which acts to smooth the distribution of slip and opening, the relative importance of which is governed by the size of the scalar smoothing factor κ; a and b are phase gradients in the x- and y-direction respectively; c are offsets to account for the unknown zero phase level (InSAR) or displacements at the reference GPS station (subscripts indicate data source) and **d** is a vector containing the observed displacements (Wright *et al.* 2004b).

Using a shear modulus of 32 GPa and a Poisson's ratio of 0.25, we solve for the best fitting opening distribution using a non-negative least-squares inversion (Bro & Jong 1997). The best fit solution depends on the size of the smoothing factor κ. High values generate an oversmooth solution with a larger misfit whereas low values cause small misfits but oscillating opening distributions. By plotting solution roughness (the mean absolute Laplacian of the slip model) against misfit, solutions that have both low misfit and roughness are selected.

To account for the different quantities and uncertainties of the GPS and InSAR data, we vary the relative weighting of each data set and assess the affect on the rms misfit (Pedersen *et al.* 2003). Increasing the weight of the GPS data relative to the InSAR shows little improvement to the fit for the GPS data but causes a significant increase in the misfit with the InSAR data. For example, setting the GPS weight to zero for the inversion of the 2006 June data set results in a rms misfit of 22.5 and 19.4 mm for the ascending and descending interferograms, respectively, and 2.7, 2.4 and 4.2 mm for the GPS in the x, y and z directions. When the InSAR data is given zero weight, the misfit to the GPS reduces to 1.1, 1.6 and 2.8 mm, respectively, but the fit to the InSAR data deteriorates significantly (300 mm, 232 mm). A good compromise can be made by giving equal weights to both data sets, whereby a good fit to both GPS and InSAR data is achieved (24, 21, 1.5, 2.0 and 4.1 mm). It is worth noting that the fit to the GPS data is good even when it has zero weight; so, it is not contributing a lot of additional information to the inversion.

3 2006–2007 DYKE SEQUENCE

3.1 2006 June intrusion

On 2006 June 17, five earthquakes of M_b 3.9–4.6 were reported by NEIC within the Dabbahu rift. The local seismic station network, deployed following the 2005 event, recorded a swarm of earthquakes (M_L 2.4–4.7) concentrated in the vicinity of the Ado'Ale volcanic complex (Keir *et al.* 2008).

Ascending and descending interferograms formed covering the June earthquake swarm (Figs 2 and 6) indicated new activity in the centre of the Dabbahu segment. Images acquired on May 20 and June 24 were used to construct a 35-d descending interferogram (Fig. 6d). A large baseline, ∼1200 m, prevents the formation of the ascending interferogram using images acquired on June 12 and July 17 on track 300. Instead, we used the interferogram from June 12 to August 21, which includes deformation from intrusions in both June and July. To isolate the signal for the June intrusion, the deformation associated with the July event was removed by subtracting the 35-d ascending interferogram from July 17 to August 21, acquired on the same track. Three of the GPS sites show relative displacements with respect to the most distant site, DA60 (Fig. 5a). The closest of these was 25 km west of the rift axis (DA25), and recorded a westward displacement of 47 mm (Fig. 6a). An epoch-by-epoch analysis of GPS data shows that the intrusion occurred in approximately 4 hr (Keir *et al.* 2009).

Deformation was concentrated in the centre of the rift segment, and the location of seismicity correlates well with the InSAR data (Keir *et al.* 2009). Surface deformation patterns are in agreement with the displacement field from the intrusion of a ∼10-km-long dyke oriented NNW–SSE. In the ascending interferogram (Fig. 6a), 19 fringes were observed on the western flank indicating a maximum line-of-site displacement of ∼54 cm towards the satellite (range decrease). On the eastern flank, a maximum range increase of ∼12 cm was observed. The asymmetric deformation pattern is a result of the viewing geometry. In the east-looking ascending

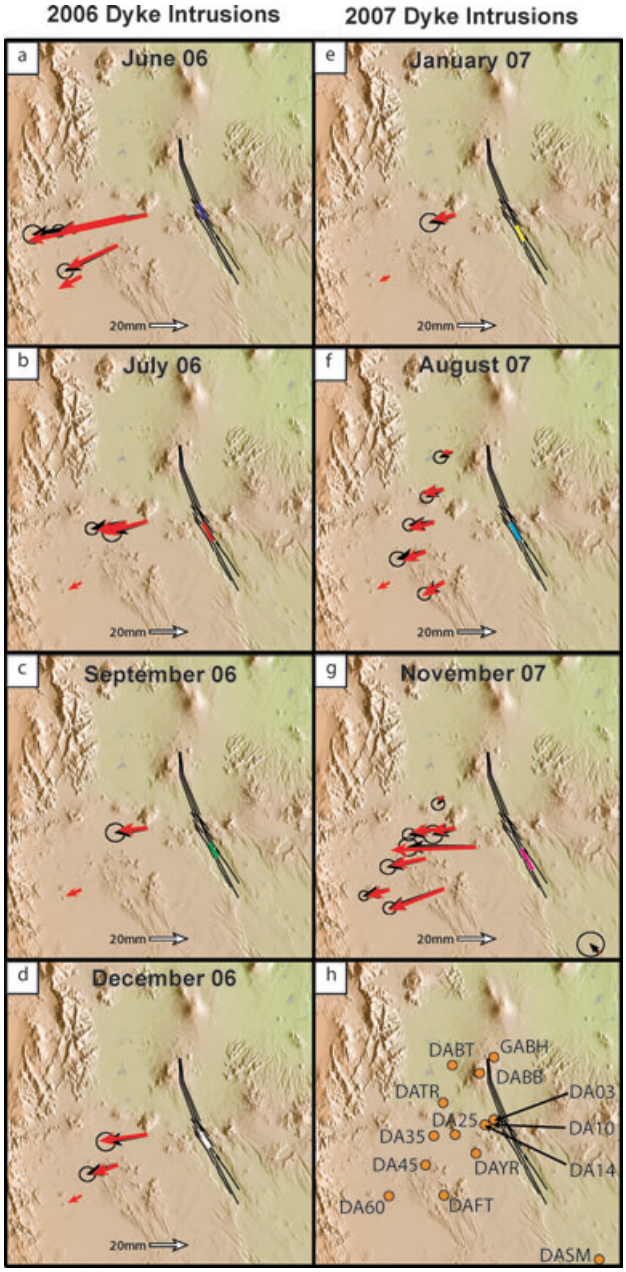

Figure 5. Observed and modelled GPS data covering each of the new dyke intrusions (a–g). Black arrows show the observed GPS displacements, with 95 per cent confidence ellipse for each of the dyke intrusions, with the offset determined during the inversion added (see Section 2.2 for details). Red arrows show the corresponding modelled displacements from the joint inversion of InSAR and GPS data. Black lines show the location of the dyke model, coloured lines show the location of the individual dykes. (h) Location of all continuous GPS sites around the Dabbahu rift segment. The number of GPS stations present varies with time as a function of deployment schedule and technical interruptions at the sites (see also Fig. 3).

interferogram (Fig. 6a), horizontal and vertical displacements to the west of the dyke are toward the satellite and sum constructively, whereas on the east side of the dyke displacement is toward the satellite in the vertical direction but away from the satellite in the horizontal. The asymmetry is reversed for the west-looking descending track (Fig. 6d), where −23 (∼65 cm) and +9 (∼19 cm) fringes were observed on the eastern and western flanks, respectively. The larger signal is mainly due to a higher incidence angle used for this acquisition (45°), making the satellite more sensitive to horizontal motion. Displacements recorded by GPS were used in a joint inversion of InSAR and GPS data. The modelled GPS displacements provide a good fit to the data and lie within the 95 per cent confidence ellipses for the GPS estimates of displacement (Fig. 5), if three additional free parameters are included to account for the motion of reference point DA60.

The best fitting model (Figs 6b, e and g) from the inversion of InSAR and GPS data obtained with a solution roughness of 1.1×10^{-5} cm km^{-2}, suggests the dyke was ∼10 km long, agreeing with observed seismicity, with a maximum opening of 2.2 m, and that normal faults slip by no more than 1.3 m. Most opening occurred between 2 and 8 km depth, with little opening below 9 km or above 1 km. A total of 0.12 km^3 of magma was intruded, only ∼5 per cent of the 2005 September intrusion, giving a geodetic moment of 5.4×10^{18} N m. Errors in opening, calculated using the Monte Carlo simulations described in Section 2.3.1, are plotted on the dyke model (Fig. 6h), revealing areas where the opening is less well constrained. The 1-σ errors in the inversion are less than 22 cm throughout the model, with maximum errors occuring in regions of incoherence in the InSAR data. The model explains most of the deformation with rms misfit to the LOS data of 21 mm (Figs 6c and f), comparable to the level of noise in the far field (∼20 mm). Larger misfits occur close to the dyke where data coherence is poor and where our simplified geometry does not fully reflect the complexity of real faults. Misfits at the northern end of the dyke occur where inflation of Dabbahu and Gabho volcanoes is not modelled. Table 2 gives values for the seismic moment, amount of opening, volume and depth for each of the dykes.

3.2 2006 July intrusion

Seismicity in the Dabbahu rift was low after the June intrusion until July 25–26, when a swarm of M_L2–3 earthquakes were recorded by our local network to the south of Ado'Ale (Keir *et al.* 2008).

Two 35-d interferograms, one ascending and one descending (Figs 7a and d), formed covering the month of July reveal the intrusion of a new dyke. The ascending interferogram, using images acquired on July 17 and August 21, has a 564 m baseline causing some coherence loss compared with the descending interferogram June 24–July 29), which has a smaller baseline of 365 m.

The intrusion was smaller in size and located to the south of the June intrusion, but the observed surface deformation was similar. The displacements are consistent with the intrusion of another dyke oriented NNW–SSE and correlates with the spatial distribution of seismicity (Keir *et al.* 2008). In the ascending interferogram (Fig. 7a), we see ∼37 cm of range decrease on the western flank and ∼8.5 cm of range increase on the eastern flank. On the descending track (Fig. 7d), ∼56 cm of displacement has occurred on the eastern flank and ∼11 cm in the west. In addition, ∼6 cm of uplift was observed at Dabbahu at the northern end of the segment. Displacement vectors at two sites, DA25 and DA35 (Fig. 5), also recorded the dyke intrusion with a westward displacement of 18 and 17 mm, respectively.

Using a solution roughness of 6.5×10^{-6} cm km^{-2}, the best fitting model (Figs. 7b, d and g) suggests a 9-km-long dyke, intruded between depths of 0 and 5 km. Maximum opening of 1.1 m occurred in the centre of the dyke and the normal faults above slipped by up to 1 m. A total volume of 0.068 km^3 was intruded (2.7 per cent of 2005 September), giving a geodetic moment of 3.2×10^{18} N m. The 1-σ error in model opening is less than 13 cm with a maximum

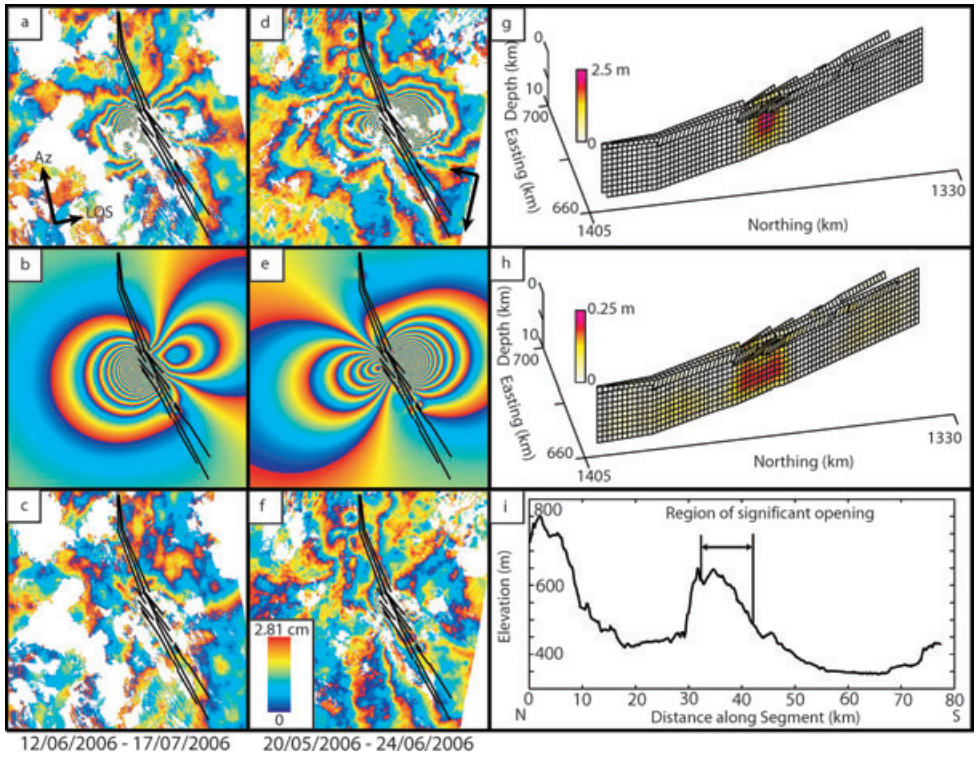

Figure 6. (a) and (d) Observed ascending and descending interferograms covering June 17 dyke intrusion. Arrows indicate the satellites flight (Az) and look (LOS) directions. (b) and (e) Simulated ascending and descending interferograms, constructed using the distributed opening model (g), described in the text. (c) and (f) Residual ascending and descending interferograms for each of the distributed opening models, generated by subtracting the model interferograms from the data. (h) 1σ error projected onto best fitting model. (i), along axis topography—black lines indicate region above significant dyke opening.

Table 2. Distributed opening model parameters for each of the dykes (see Section 2.3.2 for details). The depth range is delimited by condition that dyke opening is $\frac{1}{e}$ of the maximum.

Date	Moment (10^{18} N m)	Volume (km^3)	Max Opening (m)	Depth (km)	rms (mm)
June 2006	5.44	0.12 ± 0.01	2.2 ± 0.2	0-10	22
July 2006	3.24	0.047 ± 0.017	1.1 ± 0.1	0-6	19
September 2006	3.24	0.088 ± 0.014	1.2 ± 0.1	3-10	23
December 2006	3.05	0.058 ± 0.011	1.78 ± 0.1	1-6	27
January 2007	2.07	0.037 ± 0.013	0.7 ± 0.1	2-7	10
August 2007	2.41	0.048 ± 0.001	2.4 ± 0.1	0-3	26
November 2007	6.01	0.15 ± 0.01	1.7 ± 0.1	0-8	21

occuring in regions close to the dyke (Fig. 7h). Most of the observed deformation is explained by the model with a rms misfit of 19 mm. The largest misfits occur close to the dyke where the effect of the near-surface faults is felt. A broad residual to the north of the intrusion, most notably on the descending track (Fig. 7f), is probably a result of atmospheric noise and continued relaxation of the crust being modelled as opening. Modelled GPS displacements fit the data well and lie close to or within the error ellipse for each site (Fig. 5b).

3.3 2006 September intrusion

During 2006 August, little seismicity was observed in the Dabbahu segment. However, on 2006 September 10 a swarm of 14 M_L 2.6–3.4 earthquakes were detected near Ado'Ale (D. Keir, private communication, 2008). Ascending and descending interferograms (Figs 8a and d) formed between August 21 and September 25 and September 2 and October 7, respectively, indicate the intrusion of a third dyke, oriented NNW–SSE and located to the south of the July intrusion. The deformation was less than that caused by previous intrusions, with a maximum ∼14 cm of range decrease in the ascending interferogram and ∼19 cm in the descending. This was mirrored in the GPS data (Fig. 5c), only the station at DA25 records the intrusion showing a maximum westward displacement of ∼11 mm.

With a solution roughness of 7.1×10^{-6} cm km^{-2}, the model for the September 2006 event is able to explain most of the deformation (Figs 8b, d and g), yielding an rms misfit to LOS data of 20 mm. Maximum opening of 1.2 m occurred between 3 and 8 km depth with normal faults slipping up to a maximum of 0.5 m. The total intruded volume was 0.088 km^3, again small (3.6 per cent) relative to the event of September 2005. The moment release from the recorded earthquakes was only ∼0.1 per cent of the total geodetic moment (3.2×10^{18} N m). The model has a 1-σ error of less than 15 cm everywhere, with the largest errors occuring where displacement is greatest and further south where the model may be influenced by an atmospheric signal.

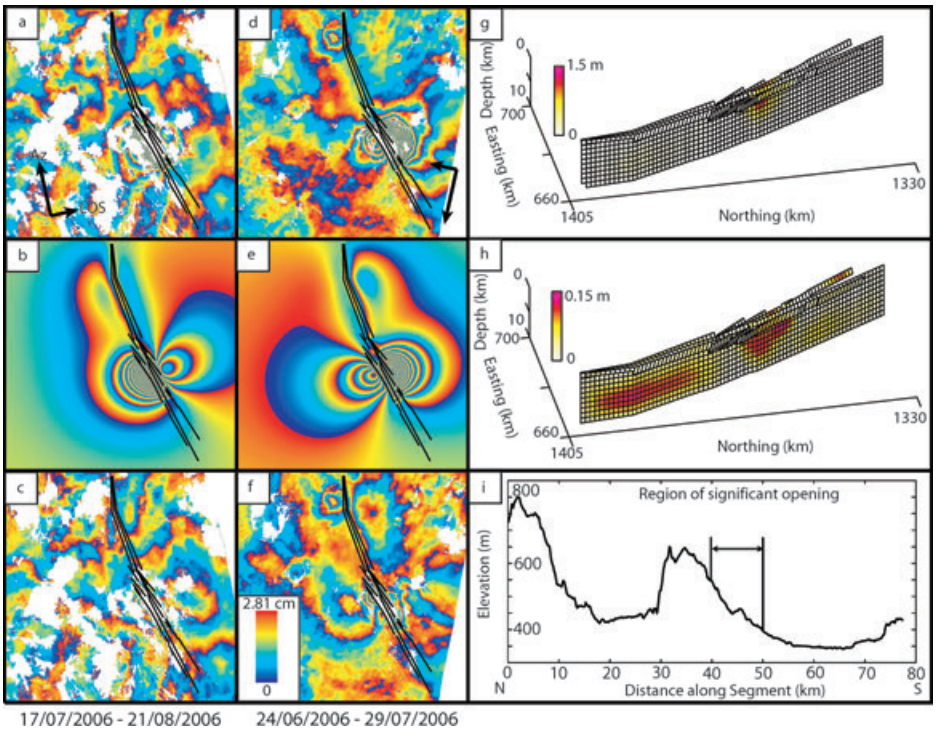

Figure 7. (a) and (d) Observed ascending and descending interferograms covering the 2006 July 24 dyke intrusion. Arrows indicate the satellites flight (Az) and look (LOS) directions. (b) and (e) Simulated ascending and descending interferograms, constructed using the distributed opening model (g), described in the text. (c) and (f) Residual ascending and descending interferograms for each of the distributed opening models, generated by subtracting the model interferograms from the data. (h) 1σ error projected onto best fitting model. (i), along axis topography—black lines indicate region above significant dyke opening.

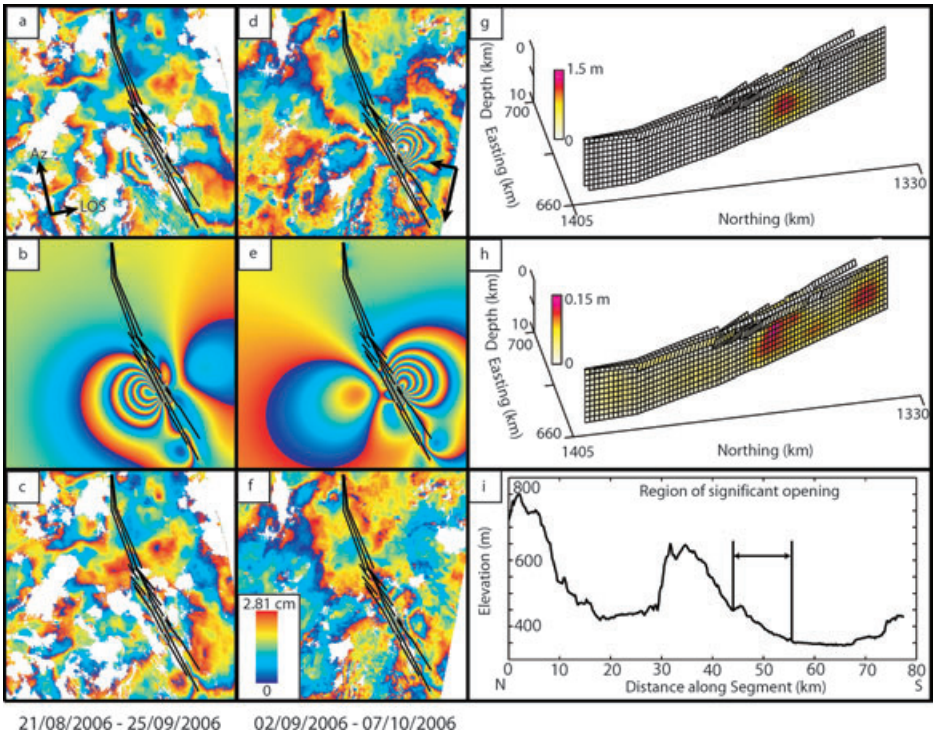

Figure 8. (a) and (d) Observed ascending and descending interferograms covering the 2006 September 10 dyke intrusion. Arrows indicate the satellites flight (Az) and look (LOS) directions. (b) and (e) Simulated ascending and descending interferograms, constructed using the distributed opening model (g), described in the text. (c) and (f) Residual ascending and descending interferograms for each of the distributed opening models, generated by subtracting the model interferograms from the data. (h) 1σ error projected onto best fitting model. (i) along axis topography—black lines indicate region above significant dyke opening.

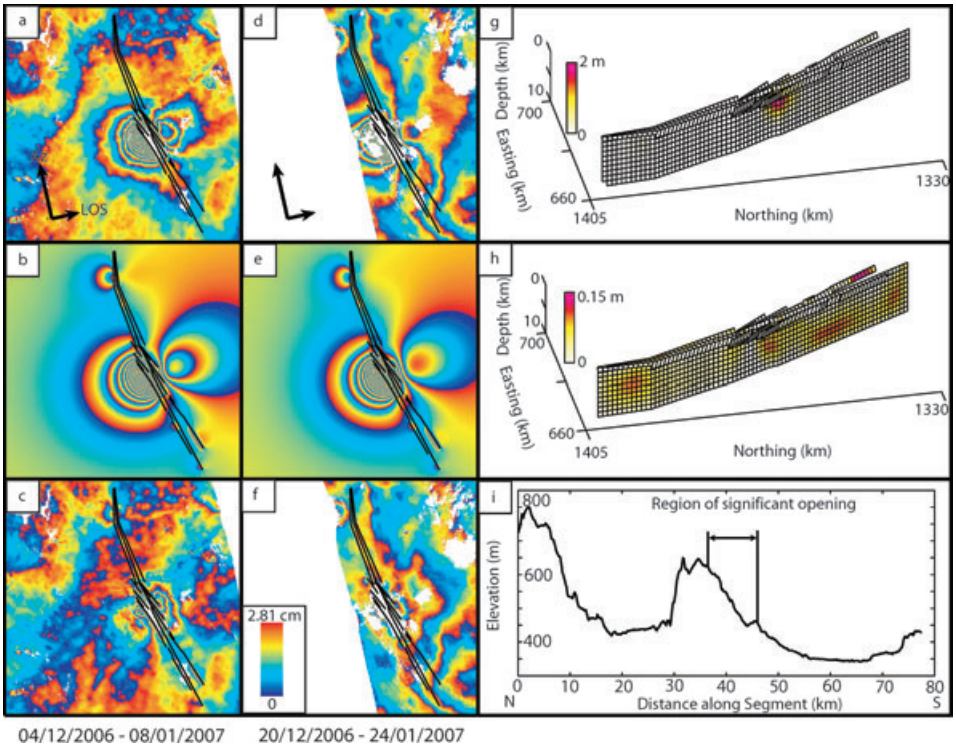

Figure 9. (a) and (d) Two ascending interferograms covering December dyke intrusion. Arrows indicate the satellites flight (Az) and look (LOS) directions. (b) and (e) Simulated ascending and descending interferograms, constructed using the distributed opening model (g), described in the text. (c) and (f) Residual ascending and descending interferograms for each of the distributed opening models, generated by subtracting the model interferograms from the data. (h) 1σ error projected onto best fitting model. (i) along axis topography—black lines indicate region above significant dyke opening.

3.4 2006 December intrusion

Surface deformation seen in interferograms covering the beginning of December reveal the intrusion of a fourth dyke. The event was captured by GPS (Fig. 5d), indicating that the intrusion occurred on December 7. Two ascending interferograms (Figs 9a and d), on tracks 300 and 28, show deformation concentrated to the north of the 2006 September event and between the intrusions of 2006 June and July. Interferograms on the descending track cover both of the intrusions in December and January, therefore only ascending interferograms isolate the event and are modelled. The pattern of deformation was similar to that observed for the intrusions in June and July; ∼50 cm of motion was detected towards the satellite with the ground moving away by ∼8.5 cm on the eastern flank.

The model for the 2006 December event suggests a 7–8 km long dyke intruded between 1 and 6 km depth. Maximum opening of 1.8 m occurred between 2 and 5 km depth and normal faults slipped by no more than 0.9 m. Approximately 0.06 km^3 of magma was intruded (3.4 per cent of 2005 September) with a geodetic moment release of 3.05×10^{18} N m. The 1σ error of the opening is less than 15 cm for the entire model, with most parts having an error of $< \sim$10 cm. The model is able to explain most of the deformation observed in the interferograms (Figs 9b and e), with an rms misfit to the LOS data of 19 mm. Greatest residuals occur close to the dyke and in the north, residuals in the north are due to the inflation of Dabbahu volcano being modelled as opening on the dyke.

3.5 2007 January intrusion

Further dyking occurred during 2007 January, located in the south of the segment. The dyke was intruded along the same section as the 2006 September event. The surface deformation was very similar in the ascending interferogram, with ∼19 cm of motion detected towards the satellite and ∼3 cm away (Fig. 10a). GPS displacements reveal that the intrusion occurred on January 14 (Fig. 5e). As for the December event, no descending interferograms can be formed, which capture this event without including the deformation from the previous intrusion.

The best fitting model, (Figs 10b and d) suggests a dyke with a maximum opening of 0.7 m between 4 and 8 km depth. The opening was 9-10 km long at depth but narrowed towards the surface where normal faults slipped by no more than 1.1 m. Only 0.045 km^3 of magma was intruded, 1.6 per cent of the volume intruded during the 2005 September event, resulting in a total geodetic moment of 2.07×10^{18} N m. The 1σ error is less than 11 cm everywhere, with the largest errors occuring close to the areas of maximum opening (Fig. 10e). High coherence and low atmospheric noise across the scene means that residuals are relatively small with an rms misfit of 10 mm to the LOS data (Fig. 10c).

3.6 2007August intrusion

Deformation in the Dabbahu segment between January and the end of 2007 July, following the January intrusion, was small and isolated around Dabbahu volcano and the centre of the rift segment. However, information given to the Geophysical Observatory in Addis Ababa reported activity in the Karbahi region, close to the Ado'Ale volcanic complex in early August. On August, local pastoralists reported seeing 'fire' and smoke in the vicinity, which continued until August 16. Hotspots associated with the eruption were detected by NASA's Moderate-resolution Imaging Spectrometer (Wright *et al.* 2004a) over this period. Ground investigations

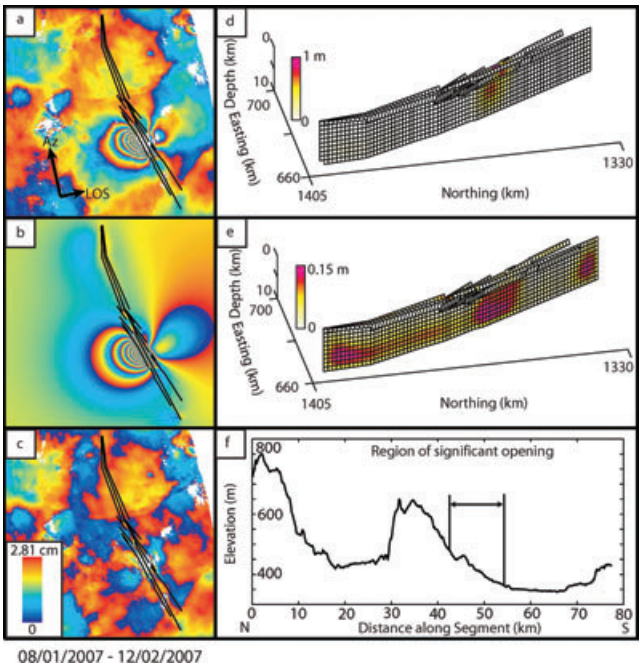

Figure 10. (a) Observed ascending interferogram covering the 2007 January dyke intrusion. Arrows indicate the satellites flight (Az) and look (LOS) directions. (b) Simulated ascending interferogram, constructed using the distributed opening model (d), described in the text. (c) Residual ascending interferogram for the distributed opening model, generated by subtracting the model interferogram from the data. (e) 1σ error projected onto best fitting model. (f) along axis topography—black lines indicate region above significant dyke opening.

carried out by a team from Addis Ababa University revealed that fresh basaltic lavas were erupted from long fissures over a total distance of ∼5 km. The observed flows travelled a few hundreds of metres from their associated fissure vents (Yirgu *et al.* 2007).

Interferograms covering the period were available on both ascending and descending tracks (Figs 11a and d) and reveal the intrusion of a dyke in the centre of the rift segment, in approximately the same location as the 2006 July dyke intrusion (Fig 7a and d). In the ascending interferogram, the ground was displaced by ∼54 cm toward the satellite on the western flank and moved away by ∼12 cm on the east side, with similar displacements observed in the descending interferogram. Hotspots and field observations of lava flows associated with the dyke were located along the southern ∼5 km of the deformation field, implying that the whole dyke did not rupture the surface.

The model provides a good fit to the LOS displacements, with an rms misfit of 22 mm. The best fitting model (Figs 11b, e and g) suggests a dyke with a maximum opening of 2.4 m, intruded between 0 and 3 km depth and with normal faults that slip by no more than 0.7 m. The dyke was 9-10 km long with more opening at the southern end in accordance with field observations that surface flows were observed in this location. A total volume of 0.06 km^3 of magma was intruded (2.4 per cent of the volume intruded during the 2005 September event) resulting in a total geodetic moment of 2.4×10^{18} N m. Assuming the eruption was 5 km long, 200 m across and no more than 2 m thick, as estimated from field observations, the total erupted volume was <0.002 km^3, only 3 per cent of the total intruded volume. The location of the dyke is very similar to the July dyke, but maximum opening has occured at a shallower depth. The intrusion is captured by multiple GPS sites around the rift and the modelled displacements provide a good fit with the data (Fig. 5f). The 1σ error is less than 15 cm everywhere, with maximum errors occuring close to the areas of greatest opening (Fig. 11h) and further north, where there is a secondary signal in the data, which may be unrelated to the dyke event.

3.7 2007 November

During 2007 September and October, little deformation was observed along the Dabbahu segment. Interferograms spanning 2007 November indicate the intrusion of a seventh dyke in the south of the segment. The event was captured in multiple interferograms (Figs 12a and b), and the available GPS data indicates that the intrusion occurred on November 12. In both the ascending and descending interferograms, up to ∼40 cm of displacement occurs towards the satellite and ∼15 cm away. At the northern end of the dyke, there was a zone of up to ∼8.5 cm of subsidence, implying that at least some of the magma may have been sourced from a shallower chamber, something that has not been observed during the previous intrusions.

The best-fitting model for the November 2007 event (Figs 12a, e and g), suggests a dyke intruded between 0 and 8 km depth, with a maximum opening of 1.7 m. Normal faults slip by no more than 1.8 m. The total intruded volume was 0.15 km^3, making it the most voluminous of the dykes since September 2005, with a geodetic moment release of 6.0×10^{18} N m. The model explains most of the observed deformation with a rms misfit to the LOS displacement of 22 mm (Figs 12c and f). The 1σ error is less than 20 cm, with maximum errors occurring close to the dyke where coherence is low. The zone of subsidence to the north of the dyke can be explained with a point pressure source (Mogi 1958), deflating by between 0.019 and 0.032 km^3 (12–14 per cent of total), at 7–10 km depth (Fig. 11g). Modelled GPS displacements fit the data well (Fig. 5g), with the exception of the station at DAYR, where we overestimate the displacement by ∼9 mm.

4 DISCUSSION

Most of the deformation associated with the 2006 June to 2007 November dyke intrusions can be explained by our simple models. The combination of seismicity, GPS and InSAR data from the Dabbahu rift make it is possible to constrain the timing of each event and estimate their displacement fields.

The pattern of dyke intrusion observed within the Dabbahu rift segment shows many temporal and spatial similarities with the 1975–1984 Krafla rifting episode in Northern Iceland, where 9 m of rift opening occurred through 20 discrete dyke intrusions (Fig. 14). To date, the intrusion of eight dykes has been observed in the Dabbahu rift segment in Afar. Seismicity associated with both the 2006 June and July dyke intrusions indicate that the intrusions occurred over several hours on June 17 and July 25, and that the dykes propagated at velocities of ∼1–2 m s^{-1} (Keir *et al.* 2008), similar to those observed during the Krafla episode (Einarsson & Brandsdóttir 1980). The total volume estimated to have been intruded during the Krafla rifting episode was ∼1.1 km^3 (Tryggvason 1984). The volume of magma intruded during 2005 September was ∼2.5 km^3 (Wright *et al.* 2006) and a further ∼0.5 km^3 was intruded between 2006 June and 2007 November.

With the exception of the 2007 November intrusion, we do not observe any subsidence in the InSAR data at the volcanic centres in the Dabbahu rift segment, following any of the intrusions

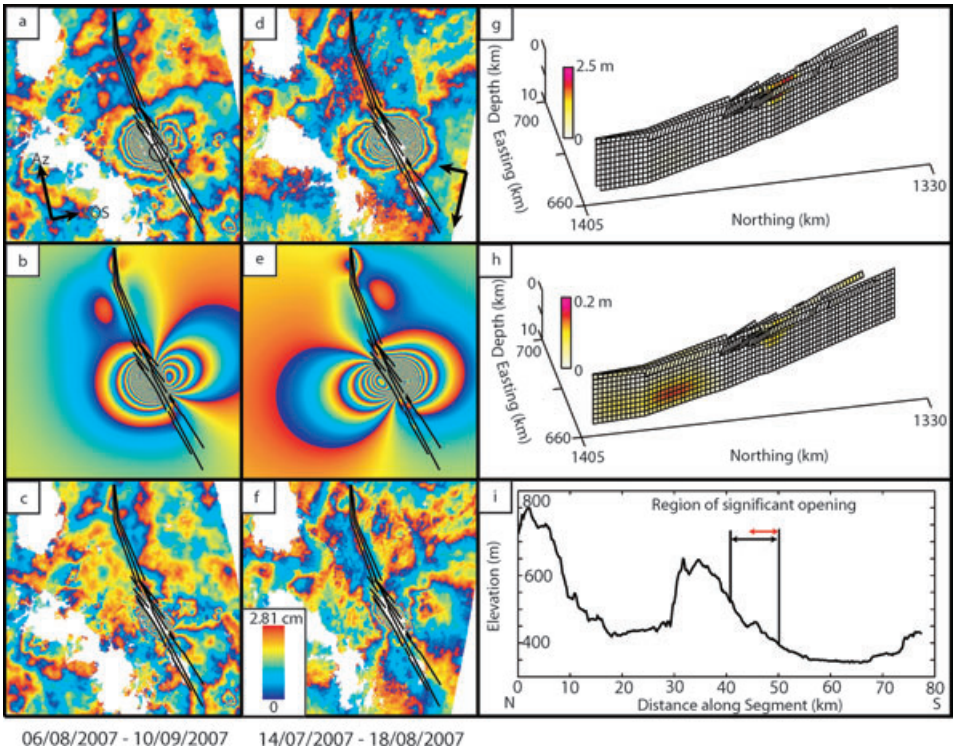

Figure 11. (a) and (d) Observed ascending and descending interferograms covering the 2007 August dyke intrusion. Arrows indicate the satellites flight (Az) and look (LOS) directions. The black circle shows the approximate location of the surface eruption. (b) and (e) Simulated ascending and descending interferograms, constructed using the distributed opening model, (g), described in the text. (c) and (f) Residual ascending and descending interferograms for each of the distributed opening models, generated by subtracting the model interferograms from the data. (h) 1σ error projected onto best fitting model. (i) along axis topography—black lines indicate region above significant dyke opening and red indicates the extent of the surface flows.

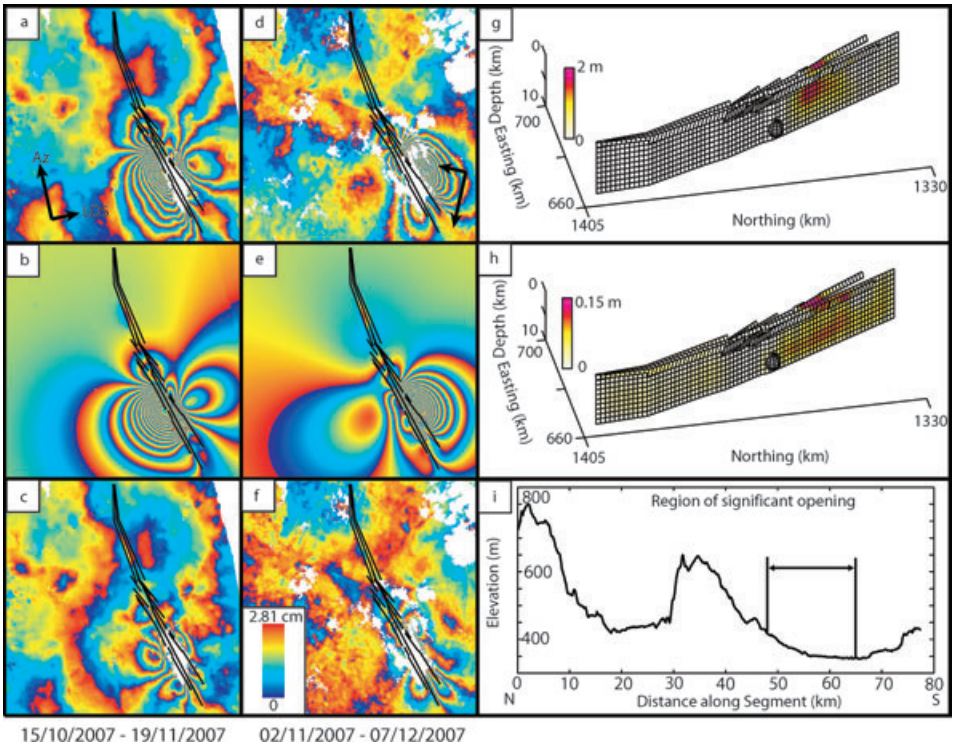

Figure 12. (a) and (d) Observed ascending and descending interferograms covering the 2007 November intrusion, arrows indicate the satellites flight (Az) and look (LOS) directions. (b) and (e) Simulated ascending and descending interferograms, constructed using the distributed opening model (g), described in the text. (c) and (f) Residual ascending and descending interferograms for each of the distributed opening models, generated by subtracting the model interferograms. (h) 1σ error projected onto best fitting model. (i) along axis topography—black lines indicate region above significant dyke opening.

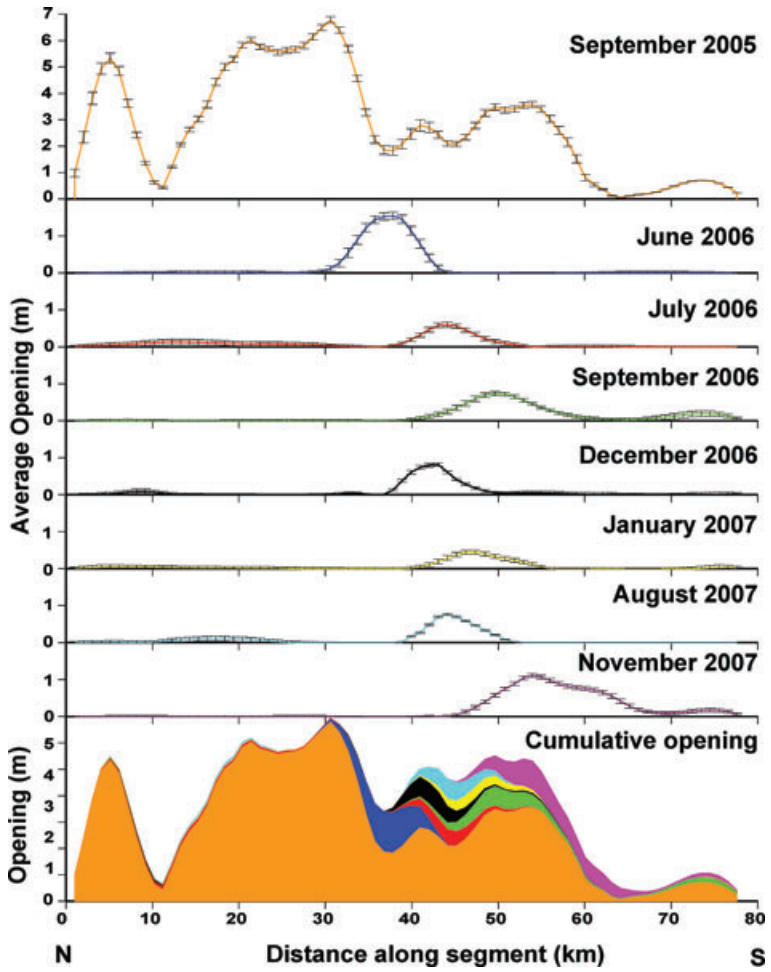

Figure 13. Depth averaged dyke opening for the top 10 km versus distance along the segment from north to south. Lines represent the average opening for each of the dyke intrusions (labelled). Solid graph shows the cumulative opening for all of the dykes, September 2005 (orange), 2005 September –2006 June (blue line), 2005 September–2006 July (red), 2005 September–2006 September (green), 2005 September–2006 December (black), 2005September–2007 January (yellow), 2005 September–2007 August(cyan) and 2005 September–2007 November (pink). The dashed line shows the 5-6 m opening envelope, area beneath the line are the regions which have not achieved 5–6 m of opening.

However, the withdrawal of magma from crustal magma chambers and the subsequent deflation of volcanic centres is frequently observed during dyke intrusions (Björnsson *et al.* 1977, 1979; Tryggvason 1980, 1984, 1994; Cervelli *et al.* 2002). During the Krafla rifting episode, intrusions were accompanied by rapid deflation of the Krafla caldera, after which inflation resumed. The primary magma chamber beneath Krafla is at about 3 km depth. Assuming that 0.12 km^3 of magma was intruded in the June 2006 dyke, the surface deformation caused by a Mogi source deflating by the same amount at 3 km depth would cause ∼3 m of surface displacement. A source located at 15 km depth would cause a maximum of ∼15 cm of subsidence over a broad area and we would expect to see some subsidence at the GPS sites 25 and 35 km away. However, this is not observed following any of the intrusions except in 2007 November when minor localized subsidence was observed at Ado'Ale silicic complex. Simple Mogi modelling for this magma chamber indicates a source located at ∼7–10 km depth, releasing a maximum of ∼0.023 km^3 of magma, only 14 per cent of the total intruded volume. Similar volume discrepancies were observed in the 2005 September intrusion in Afar, where only 0.5 km^3 of magma was sourced from the volcanoes at the north of the segment (Wright *et al.* 2006). This discrepancy could be explained by magma compressibility (Delaney & McTigue 1994), incorrect Poissons ratio (Johnson *et al.* 2000) or the difference in compliance between the magma chamber and the dyke (Rivalta & Segall 2008). Another possibility could be that the magma supply rate is equal to the drainage rate during the intrusions, therefore no deflation of the chamber would be observed (Mériaux & Jaupart 1995), or that the magma source could be at depth such that we do not observe any measurable signal at the surface. The presence of a deep source situated at the crust–mantle boundary beneath the Krafla volcanic system has been suggested by de Zeeuw-van Dalfsen *et al.* (2004) and cannot be ruled out in the Dabbahu segment. The modelled vertical displacment at DA25, associated with the 2006 dyke June, is 24 mm, whereas the observed displacement at the same site was ∼15 mm (±5.8 mm). If we assume that the difference in vertical signal is the result of a deflating body and take into account the vertical offset at DA60, then a point source deflating by 0.12 km^3 would have to be between ∼33 and ∼160 km deep.

Simulations of dyke intrusions indicate that dyke propagation is largely controlled by the difference between tectonic stress and magma pressure (Buck *et al.* 2006). Maximum opening during the 2005 September event occurred north of Ado'Ale, locally relieving the tectonic stress in the upper crust. Fig. 13 shows the depth

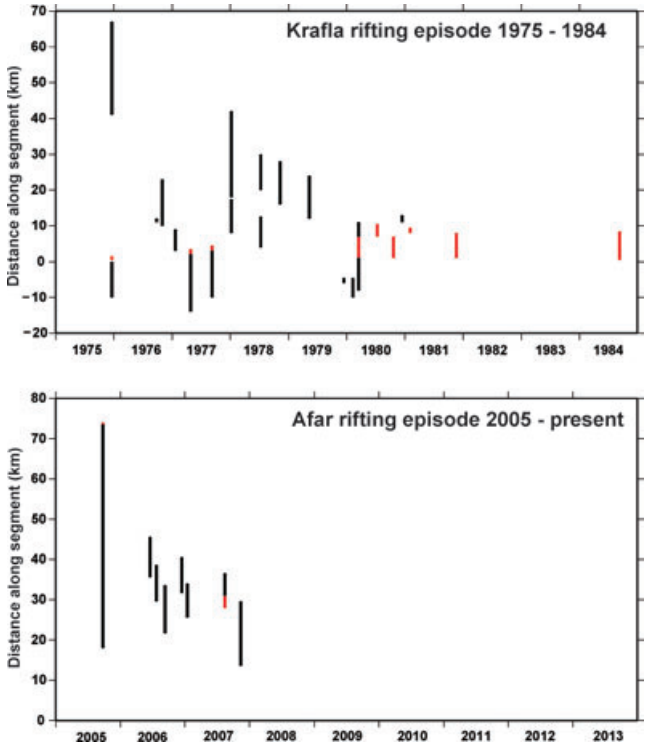

Figure 14. Along-strike movement of dyking activity with time during the 1974–1989 Krafla episode, (after Einarsson 1991) and for the ongoing Afar episode. Black lines show the length of each dyke without extrusion of lava, red lines show length of dyke with extrusion.

averaged, cumulative dyke opening versus distance along the segment. The new dyke intrusions have largely been intruded into regions where the opening associated with the 2005 September event (orange line) was the lowest and therefore where the tectonic stresses probably remained high. The new intrusions follow a similar pattern, dykes with lower amounts of opening are intruded again, for example, the dykes in 2006 July and September are re-intruded at different depths during 2007 August and January, respectively (Fig. 13). In addition, to the north and south of Ado'Ale, the orientation of the segment changes relative to the regional extension direction. South of Ado'Ale the segment is near orthogonal to the regional extension direction (NW–SE). However, to the north, the segment swings by ∼20° to a more northerly orientation, where it becomes more oblique, approximately 60°, to the regional extension direction (Rowland *et al.* 2007), causing a difference in stress to the north and south of Ado'Ale.

Dyking in Afar has largely been at depth, with only one dyke resulting in a surface eruption. In comparison, nine of the 20 dykes intruded during the Krafla rifting episode resulted in surface basaltic flows, with three of those occurring in the first 2 yr. Models of dyke propagation following the Krafla rifting episode (Buck *et al.* 2006) indicate that extrusive eruptions will only occur when the principal horizontal stress is equal to or greater than the vertical stress, in other words, when it becomes easier for the magma to propagate vertically rather than laterally. In Afar, only the southern ∼5 km of the 2007 August dyke intrusion results in the extrusion of basaltic material, implying that the tectonic stress was locally relieved during the intrusion. In addition, the topography at the southern end of the dyke is likely to have had an influence on where the extrusion occurred. The southern end of the dyke corresponds to a topographic low (Fig. 11i). Assuming the dyke is intruded at a shallow depth, as with the July intrusion, the ∼200 m lower topography may have enabled the dyke to intercept the surface in this region.

It is clear from the available data that magma intruded during the 2006 June to 2007 November dykes was not sourced from either of the volcanoes at the northern end of the segment, Dabbahu and Gabho, which provided some of the magma for the 2005 intrusion. Lateral migration of seismicity away from Ado'Ale during the 2006 June and July intrusions (Keir *et al.* 2008), the broad zone of uplift observed in both InSAR and GPS data prior to the June intrusion, and the subsidence observed in 2007 November point towards a magma source located beneath the Ado'Ale volcanic complex.

Observations from the Krafla rifting episode (Fig. 14) suggests that dyking in the Dabbahu segment will continue while a magma source persists and until the tectonic stress has been relieved. It is evident that new dyking occurs in regions where less opening has occurred in previous intrusions (Fig. 13). Assuming that the tectonic stress along the segment is smooth spatially, we expect 5–6 m of opening everywhere along the segment. Thus, if the pattern of intrusion continues, then we expect that any new dykes will be intruded into regions along the segment that have yet to experience ∼6 m of opening. It is therefore likely that any new dyking will be focused in the area of current activity south of Ado'Ale and in the region in the north of the segment, ∼5–20 km south of Dabbahu volcano, or possibly on the neighbouring segments, Hararo in the south and Alayta in the north.

5 CONCLUSIONS

We have presented new geodetic data from Envisat interferometry to determine dyking models for a sequence of seven dykes in Northern Afar, Ethiopia. The sequence of dyking is ongoing in the Dabbahu rift segment and the intrusions are shown to be similar to the 9 yr 1975–1984 Krafla rifting episode. Distributed opening models indicate that the total volume intruded from the 2006 June–2007 November dyke sequence is ∼25 per cent of the 2005 September intrusion. The location of new dyking appears to be related to stress levels in the crust, with new dykes progresively being intruded into areas where less opening occurred during the 2005 September intrusion. Inflation around the Ado'Ale volcanic complex prior to the intrusions, lateral migration of seismicity and geodetic data, all indicate the presence of a magma source in the centre of the rift segment. With a continued supply of melt, dyking will continue in the Dabbahu rift segment until the tectonic stress is relieved.

ACKNOWLEDGMENTS

We'd like to thank the Geophysical Observatory of Addis Ababa University, the Afar Regional government and the Ethiopian Ministries of Capacity Building and of Mines and Energy for all their help and support. Our work is supported by NERC grants NE/D008611/1, NE/D01039X/1 and NE/E007414/1, NSF grants EAR-0635789 and EAR-0613651, a NERC-COMET studentship to IJH and a Royal Society University Research Fellowship to TJW. Radar data is from European Space Agency. Thanks to Greg Houseman, Dan Morgan and Eleonora Rivalta provided valuable comments on early drafts of the manuscript and to Juliet Biggs and Kurt Feigl for their insightful reviews that have helped improve the manuscript.

REFERENCES

Abdallah, A. *et al.*, 1979. Relevance of Afar seismicity and volcanism to the mechanics of accreting plate boundaries, *Nature,* **282,** 17–23.

Ayele, A. *et al.*, 2007. The volcano-seismic crisis in Afar, Ethiopia, starting September 2005, *Earth planet. Sci. Lett.,* **255,** 177–187.

Barberi, F. & Varet, J., 1975. Recent volcanic units of Afar and their structural significance, in *Afar Depression of Ethiopia: Proceedings of an International Symposium on the Afar Region and Related Rift Problems,*Vol. 1, pp. 174–178, Schweizerbart, Stuttgart.

Barberi, F., Tazieff, H. & Varet, J., 1972. Volcanism in the Afar depression: its tectonic and magmatic significance, *Tectonophysics,* **15,** 19–29.

Barrat, J., Joran, J., Taylor, R., Fourcade, S., Nesbitt, R. & Jahn, B., 2003. Geochemistry of basalts from Manda Hararo, Ethiopia: LREE-depleted basalts in Central Afar, *Lithos,* **69,** 1–13.

Bastow, I., Nyblade, A.A., Stuart, G.W., Rooney, T.O. & Benoit, M.H., 2008. Upper mantle seismic structure beneath the Ethiopian hot spot: rifting at the edge of the African low-velocity anomaly, *Geochem, Geophys, Geosyst,* **9**, Q12022.

Benoit, M.H., Nyblade, A.A., VanDecar, J.C. & Gurrola, H., 2003. Upper mantle *P* wave velocity structure and transition zone thickness beneath the Arabian Shield, *Geophys. Res. Lett.,* **30**, No. 10, 1531, doi:10.1029/2002GL016436.

Benoit, M.H., Nyblade, A.A. & VanDecar, J.C., 2006. Upper mantle *P* wave speed variations beneath Ethiopia and the origin of the Afar Hotspot, *Geology,* **34**(5), 329–332.

Berckhemer, H. *et al.*, 1975. *Deep Seismic Soundings of the Afar Region and on the Highland of Ethiopia,* pp. 89–107, Schweizerbart, Stuttgart.

Björnsson, A., Saemundsson, K., Einarsson, P., Tryggvason, E. & Gronvald, K., 1977. Current rifting episode in North Iceland, *Nature,* **266,** 318–323.

Björnsson, A., Johnsen, G., Sigurdsson, S., Thorbergsson, G. & Tryggvason, E., 1979. Rifting of a plate boundary in North Iceland 1975-1978, *J. geophys. Res.,* **84,** 3029–3038.

Bro, R. & Jong, S.D., 1997. A fast non-negativity-constrained least squares algorithm, *J. Chemometrics,* **11,** 392–401.

Buck, W.R., Einarsson, P. & Brandsdóttir, B., 2006. Tectonic stress and magma chamber size as controls on dike propagation: Constrints from the 1975–1984 Krafla rifting episode, *J. geophys. Res.,* **111,** B12404, doi:10.1029/2005JB003879.

Cattin, R., Doubré, C., Chabalier, J.B., King, G., Vigny, C., Avouac, J.P. & Ruegg, J.C., 2005. Numerical modelling of quaternary deformation and post-seismic displacement in the Asal-Ghoubbet rift (Djibouti, Africa), *Earth planet. Sci. Lett.,* **239,** 352–367.

Cervelli, P., Segall, P., Amelung, F., Garbeil, H., Meertens, C., Owen, S., Miklius, A. & Lisowski, M., 2002. The 12 September 1999 Upper East Rift Zone dike intrusion at Kilauea Volcano, Hawaii, *J. geophys. Res.,* **107,** B7.

Chu, D. & Gordon, R.G., 1998. Current plate motions across the Red Sea, *Geophys. J. Int.,* **135**(2), 313–328.

de Zeeuw-van Dalfsen, E., Pedersen, R., Sigmundsson, F. & Pagli, C., 2004. Satellite radar interferometry 1993–1999 suggests deep accumulation of magma near the crust–mantle boundary at the Krafla volcanic system, Iceland, *Geophys. Res. Lett.,* **31,** 13611, doi:10.1029/2004GL020059.

Delaney, P. & McTigue, D., 1994. Volume of magma accumulation or withdrawal estimated from surface uplift or subsidence, with application to the 1960 collapse of Kilauea Volcano, *Bull. Volcanol,* **56,** 417–424.

Delaney, J.R. *et al.*, 1998. The quantum event of oceanic crustal accretion: Impacts of Diking at Mid-Ocean Ridges, *Science,* **281,** 222–230.

Ebinger, C.J. & Sleep, N.H., 1998. Cenozoic magmatism throughout east Africa resulting from impact of a single plume, *Nature,* **395,** 788–791.

Ebinger, C., Keir, D., Ayele, A., Belachew, M., Calais, E., Campbell, E. & Buck, R., 2008. Magma intrusion and faulting processes in a zone of continental rupture: seismicity of the Dabbahu (Afar) rift, *Geophys. J. Int.,* **176**(3), 1138–1152.

Einarsson, P., 1991. The Krafla rifting episode 1975–1989, in *Náttúra Mývatns (The Nature of Lake Myvatn),* pp. 97–139, Icelandic Nature Sci. Soc., Reykjavík.

Einarsson, P. & Brandsdóttir, 1980. Seismological evidence for lateral magma intrusion during the 1978 deflation of the Krafla volcano in NE-Iceland, *J. geophys. Res.,* **47,** 160–165.

Farr, T. & Kobrick, M., 2000. Shuttle Radar Topography Mission produces a wealth of data, *EOS, Trans. Am. geophys. Un.,* **81,** 583–585.

Goldstein, R.M. & Werner, C.L., 1998. Radar interferogram filtering for geophysical applications, *Geophys. Res. Lett.,* **25**(21), 4035–4038.

Goldstein, R.M., Zebker, H.A. & Werner, C.L., 1988. Satellite radar interferometry: two-dimensional phase unwrapping, *Radio Sci.,* **23**(4), 713–720.

Hayward, N.J. & Ebinger, C.J., 1996. Variations in the along-axis segmentation of the Afar Rift System, *Tectonics,* **15,** 244–257.

Hofmann, C., Courtillot, V., Feraud, G., Rochette, P., Yirgu, G., Ketefo, E. & Pik, R., 1997. Timing of the Ethiopian flood basalt event and implications for plume birth and global change, *Nature,* **389**(6653), 838–841.

Johnson, D., Sigmundsson, F. & Delaney, P., 2000. Comment on "Volume of magma accumulation or withdrawal estimated from surface uplift or subsidence, with the application to the 1960 collapse of Kilauea Volcano" by P.T. Delaney and D.F. Mctigue, *Bull. Volcanol.,* **61,** 491–493.

Jónsson, S., Zebker, H., Segall, P. & Amelung, F., 2002. Fault slip distribution of the 1999 M_w 7.1 Hector Mine, California, earthquake, estimated from satellite radar and GPS measurements, *Bull. seism. Soc. Am.,* **92,** 1377–1389.

Keir, D. *et al.*, 2009. Evidence for focused magmatic accretion at segment centers from lateral dike injections captured beneath the Red Sea rift in Afar, *Geology,* **37**(1), 59–62.

King, R.W. & Bock, Y., 2005. *Documentation for the GAMIT GPS Processing Software Release 10.2,* Massachusetts Institute of Technology, Cambridge, USA.

Kreemer, C., Holt, W.E. & Haines, A.J., 2005. An integrated global model of present-day plate motions and plate boundary deformation, *Geophys. J. Int.,* **154,** 8–34.

Makris, J. & Ginzburg, A., 1987. The Afar Depression: transition between continental rifting and sea-floor spreading, *Tectonophysics,* **141,** 199–214.

Manighetti, I. *et al.*, 1998. Propagation of rifting along the Arabia–Somalia plate boundary: Into Afar, *J. geophys. Res.,* **103**(B3), 4947–4974.

Massonnet, D. & Feigl, K.L., 1998. Radar interferometry and its application to changes in the Earth's surface, *Rev. Geophys.,* **36,** 441–500.

Mériaux, C. & Jaupart, C., 1995. Simple fluid dynamic models of volcanic rift zones, *Earth planet. Sci. Lett.,* **136,** 223–240.

Mogi, K., 1958. Relations between the Eruptions of Various Volcanoes and the Deformations of the Ground Surfaces around them, *Bull., Earthq. Res. Inst.,* **239,** 352–367.

Okada, Y., 1985. Surface deformation due to shear and tensile faults in a half-space, *Bull. seism. Soc. Am.,* **75,** 1135–1154.

Parsons, B. *et al.*, 2006. The 1994 Sefidabeh (eastern Iran) earthquakes revisited: new evidence from satellite radar interferometry and carbonate dating about the growth of an active fold above a blind thrust fault, *Geophys. J. Int.,* **164,** 202–217.

Pedersen, R., Jónsson, S., Árnadóttir, T., Sigmundsson, F. & Feigl, K.L., 2003. Fault slip distribution of two June M_W6.5 earthquakes in South Iceland estimated from joint inversion of InSAR and GPS measurements, *Earth planet. Sci. Lett.,* **213,** 487–502.

Press, W.H., Flannery, B.P., Teukolsky, S.A. & Vetterling, W.T., 1986. *Numerical Recipes,* Cambridge University Press, Cambridge.

Rivalta, E. & Segall, P., 2008. Magma compressibility and the missing source for some dyke intrusions, *Geophys. Res. Lett.,* **35,** doi:10.1029/2007GL032521.

Rosen, P.A., Hensley, S., Peltzer, G. & Simons, M., 2004. Updated repeat orbit interferometry package released, *EOS, Trans. Am. geophys. Un.,* **85**(5), 35, doi:10.1029/2004EO050004.

Rowland, J.V., Baker, E., Ebinger, C.J., Keir, D., Kidane, T., Biggs, J., Hayward, N. & Wright, T.J., 2007. Fault growth at a nascent slow-spreading ridge: 2005 Dabbahu rifting episode, Afar, *Geophys. J. Int.,* **171,** 1226–1246.

Schilling, J.G., Kingsley, R., Hanan, B. & McCully, B., 1992. Nd-Sr-Os isotropic variations along the Gulf of Aden: evidence for mantle-plume lithosphere interaction, *J. geophys. Res.,* **97,** 10 927–10 966.

Stuart, G., Bastow, I. & Ebinger, C., 2006. Crustal structure of the northern Main Ethiopian Rift from receiver function studies, in *The Afar Volcanic Province within the East African Rift System,* Geological Society, London, Special Publications, The Geological Society of London.

Tiberi, C., Ebinger, C., Ballu, V., Stuart, G. & Oluma, B., 2005. Inverse models of gravity data from the Red Sea - Aden -East African Rift triple junction zone, *Geophys. J. Int.,* **163,** 775–787.

Tryggvason, E., 1980. Subsidence events in the Krafla area, North Iceland, *J. Geophys.,* **47,** 141–153.

Tryggvason, E., 1984. Widening of the Krafla fissure swarm during the 1975-1981 Volcano-tectonic episode, *Bull. Volcanol.,* **47**(1), 47–69.

Tryggvason, E., 1994. Surface deformation at the Krafla volcano, North Iceland, 1982-1992, *Bull. Volcanol,* **56,** 98–107.

Vigny, C., Huchon, P., Khanbari, J.C. & Asfaw, L.M., 2006. Confirmation of Arabia plate slow motion by new GPS data in yemen, *J. geophys. Res.,* **111**, B02402.

Vigny, C. *et al.*, 2007. Twenty-five years of geodetic measurements along the Tadjoura–Asal rift system, Djibouti, East Africa, *J. geophys. Res.,* **112**, B06410.

Wolfenden, E., Ebinger, C., Yirgu, G., Deino, A. & Ayalew, D., 2004. Evolution of the northern Main Ethiopian rift: birth of a triple junction, *Earth planet. Sci. Lett.,* **224,** 213–228.

Wright, T.J., Lu, Z. & Wicks, C., 2003. Source model for the M_w 6.7, 23 October 2002, Nenana Mountain Earthquake (Alaska) from InSAR, *J. geophys. Res.,* **30**(18), 1974, doi:10.1029/2003GL1018014.

Wright, T.J., Parsons, B.E., Jackson, J.A., Haynes, M., Fielding, E.J. & England, P.C., 1999. Source parameters of the 1 October 1995 Dinar (Turkey) earthquake from SAR interferometry and seismic bodywave modelling, *Earth planet. Sci. Lett.,* **172,** 23–37.

Wright, R., Flynn, L.P., Garbeil, H., Harris, A.J.L. & Pilger, E., 2004a. MODVOLC: near-real-time thermal monitoring og global volcanism, *J. Volcanol. Geotherm. Res.,* **135,** 29–49.

Wright, T.J., Lu, Z. & Wicks, C., 2004b. Constraining the slip distribution and fault geometry of the M_W 7.9, 3 November 2002, Denali Fault Earthquake with Interferometric Synthetic Aperture Radar and Global Positioning System data, *Bull. seism. Soc. Am.,* **94**(6B), 175–189.

Wright, T.J., Ebinger, C., Biggs, J., Ayele, A., Yirgu, G., Keir, D. & Stork, A., 2006. Magma-maintained rift segmentation at continental rupture in the 2005 Afar dyking episode, *Nature,* **442,** 291–294.

Yirgu, G., Ayele, A. & Ayalew, D., 2006. Recent seismovolcanic crisis in northern Afar, Ethiopia, *EOS, Trans. Am. geophys. Un.,* **87**(33), 325–336.

Yirgu, G., Ayele, A., Fisseha, S., Chernet, T. & Damtev, A.K., 2007. Afar field trip preliminary report, available at http://www.see.leeds.ac.uk/afar/afar_text/preliminary_report.pdf.